INTERNATIONAL JOURNAL OF ROBUST AND NONLINEAR CONTROL
Int. J. Robust Nonlinear Control 2010; **20**:873–891
Published online 22 June 2009 in Wiley InterScience (www.interscience.wiley.com). DOI: 10.1002/rnc.1476

Robust MIMO disturbance observer analysis and design with application to active car steering

Bilin Aksun Güvenç[1], Levent Güvenç[1,*,†] and Sertaç Karaman[2]

[1]*Department of Mechanical Engineering, Automotive Control and Mechatronics Research Center, İstanbul Technical University, Istanbul, Turkey*
[2]*Laboratory for Information and Decision Systems, Massachusetts Institute of Technology, MA, U.S.A.*

SUMMARY

A multi-input–multi-output extension of the well-known two control degrees-of-freedom disturbance observer architecture that decouples the problem into single-input–single-output disturbance observer loops is presented in this paper. Robust design based on mapping D-stability and the frequency domain specifications of weighted sensitivity minimization and phase margin bound to a chosen controller parameter space is presented as a part of the proposed design approach. The effect of the choice of disturbance observer Q filter on performance is explained with a numerical example. This is followed by the use of structured singular values in the robustness analysis of disturbance observer controlled systems subject to structured, real parametric and mixed uncertainty in the plant. A design and simulation study based on a four wheel active car steering control example is used to illustrate the methods presented in the paper. Copyright © 2009 John Wiley & Sons, Ltd.

Received 27 February 2007; Revised 6 February 2009; Accepted 19 April 2009

KEY WORDS: disturbance observer; parameter space methods; car steering; real parametric uncertainty; structured singular value analysis; robust performance; robust stability

1. INTRODUCTION

The disturbance observer is a specific method of designing a two degree-of-freedom control architecture to achieve insensitivity to modeling error and disturbance rejection [1, 2]. It has been used successfully in a variety of motion control applications including high-speed direct drive positioning in [3] and friction compensation in [4]. The augmentation of a plant with the disturbance observer (see Figure 1) forces it to behave like its nominal (or desired) model within the bandwidth of the disturbance observer. The feedback controller for this augmented plant is then designed simply based on the nominal (or desired) plant model. The model regulation of the disturbance observer is achieved by first comparing the actual input to the plant with the input that should have been applied to obtain the measured output based on the nominal knowledge of the plant, and then by passing the difference through a positive feedback loop.

Most of the disturbance observer applications available in the literature are for single-input–single-output (SISO) plants. For application to multi-input–multi-output (MIMO) plants, a decentralized control architecture that reduces the MIMO problem to several SISO loops is proposed here. Since the MIMO disturbance observer was formulated for square systems, a four

*Correspondence to: Levent Güvenç, Department of Mechanical Engineering, Automotive Control and Mechatronics Research Center, İstanbul Technical University, Istanbul, Turkey.
†E-mail: guvencl@itu.edu.tr

Copyright © 2009 John Wiley & Sons, Ltd.

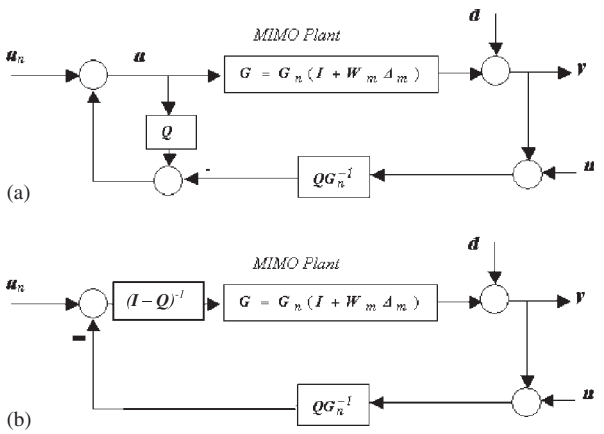

Figure 1. Plant with disturbance observer compensation (a) and equivalent block diagram (b).

wheel car steering problem which has two inputs and two outputs is chosen as the application example in this paper.

Along with its desirable model regulation and disturbance rejection properties, the disturbance observer also introduces stability and stability robustness problems due to its use of feedback. It is a standard practice to use an unstructured description of model uncertainty and low pass filter, the disturbance observer output, to avoid stability robustness problems at high frequencies corresponding to unmodeled dynamics. Many problems (see for example [5, 6]) involve well-defined real parametric uncertainty in our knowledge of the plant. The conventional stability robustness analysis based on unstructured uncertainty becomes conservative in such cases. Structured singular value (SSV) analysis is therefore proposed and used in this paper to investigate the effect of mixed parametric/complex uncertainty on the stability and performance robustness of MIMO disturbance observer compensated systems. Robust design based on mapping D-stability, frequency domain weighted sensitivity bound and phase margin bound to a chosen controller parameter space, is developed and presented in the paper.

The organization of the rest of the paper is as follows. The disturbance observer is introduced and its proposed MIMO form is presented in Section 2. The proposed design procedures are presented in Sections 3 and 4. The results on real and mixed SSV-based stability robustness analysis and mixed SSV-based performance robustness analysis are given in Section 5. A design example and a simulation study of four wheel car steering control for active yaw stabilization are used as an illustrative example in Sections 6 and 7, respectively. The paper ends with conclusions.

2. MIMO DISTURBANCE OBSERVER

The MIMO disturbance observer is developed here for plants where the desired dynamics is decoupled. There is a wealth of practical applications where this is true, the application example presented later in the paper being one of them. There are also important pitfalls of the approach presented here which are pointed out up front. These pitfalls are that a centralized MIMO decoupling disturbance observer is not presented, that the proposed method is not applicable to non-square MIMO systems and to systems where decoupled loops (i.e. a diagonal MIMO transfer function matrix) are not desired.

Consider plant $\mathbf{G}$ with multiplicative model error $\mathbf{W_m\Delta_m}$ and external disturbance $\mathbf{d}$. Its input–output relation can be expressed as

$$\mathbf{y}=\mathbf{Gu}+\mathbf{d}=(\mathbf{G_n}(\mathbf{I}+\mathbf{W_m\Delta_m}))\mathbf{u}+\mathbf{d} \tag{1}$$

where $\mathbf{G_n}$ are the nominal (or desired) model of the plant and $\mathbf{I}$ is the identity matrix of appropriate dimensions. $\mathbf{G}$ and $\mathbf{G_n}$ are square transfer function matrices with m inputs and m outputs and $\mathbf{G_n}$ is chosen to be nonsingular. $\mathbf{G_n}$ is chosen as a diagonal matrix in a decoupling type design as

$$\mathbf{G_n}(s)=\mathbf{diag}\{G_{n1}(s), G_{n2}(s), \ldots, G_{nm}(s)\} \tag{2}$$

This paper treats mainly the MIMO disturbance observer control where the desired dynamics of the plant means a decoupled system which is the rationale behind the choice of the form in Equation (2) for the desired dynamics $\mathbf{G_n}$. Consequently, the MIMO loops of the disturbance observer architecture will become weakly coupled SISO loops which are designed separately as if they were separate SISO loops. The main limitation of the approach will be due to actuator

Copyright © 2009 John Wiley & Sons, Ltd.

DOI: 10.1002/rnc

bandwidth and saturation limits as is true in any control system. The aim in disturbance observer design is to obtain

$$\mathbf{y}=\mathbf{G_n u_n} \tag{3}$$

as the input–output relation in the presence of model uncertainty and external disturbance. $\mathbf{u_n}$ in (3) is the command input signal in Figure 1. In disturbance observer design, the aim called model regulation and specified in (3) is achieved by treating the external disturbance and model uncertainty as an extended disturbance $\mathbf{e}$ and solving for it as

$$\mathbf{y}=\mathbf{G_n u}+(\mathbf{G_n W_m \Delta_m u}+\mathbf{d})=\mathbf{G_n u}+\mathbf{e} \tag{4}$$

$$\mathbf{e}=\mathbf{y}-\mathbf{G_n u} \tag{5}$$

and using $\mathbf{u}$ and $\mathbf{u_n}$ according to

$$\mathbf{u}=\mathbf{u_n}-\mathbf{G_n^{-1}e}=\mathbf{u_n}-\mathbf{G_n^{-1}y}+\mathbf{u} \tag{6}$$

to cancel the effect of the extended disturbance $\mathbf{e}$ in (4). Note that the extended disturbance $\mathbf{e}=\mathbf{G_n W_m \Delta_m u}+\mathbf{d}$ in Equations (4) and (5) includes the effects of both plant modeling error including deviation from the desired decoupled dynamics represented by $\mathbf{\Delta_m}$ and disturbances represented by $\mathbf{d}$. $\mathbf{G_n^{-1}}$ corresponding to $\mathbf{G_n}$ in (2) is

$$\begin{aligned}\mathbf{G_n^{-1}}(s)&=\mathbf{diag}\left\{\frac{1}{G_{n1}(s)},\frac{1}{G_{n2}(s)},\ldots,\frac{1}{G_{nm}(s)}\right\}\\&=\mathbf{diag}\left\{\frac{1}{G_{ni}(s)}\right\}\end{aligned} \tag{7}$$

and has noncausal transfer functions $1/G_{ni}(s):i=1,\ldots,m$ unless $G_{ni}(s):i=1,\ldots,m$ are biproper. Since this is usually not the case, $\mathbf{G_n^{-1}}$ is multiplied by a diagonal matrix of unity gain low pass filters

$$\begin{aligned}\mathbf{Q}(s)&=\mathbf{diag}\{Q_1(s),Q_2(s),\ldots,Q_m(s)\}\\&=\mathbf{diag}\{Q_i(s)\}\end{aligned} \tag{8}$$

such that $\mathbf{QG_n^{-1}}$ and hence $Q_i(s)/G_{ni}(s):i=1,\ldots,m$ are all causal. Another use of the $Q_i(s)$ filters is to limit the compensation to a pre-selected low-frequency range (in an effort not to overcompensate at high frequencies and to avoid stability robustness problems). The feedback signals in (6) are thus pre-multiplied by $\mathbf{Q}$. In this case, the implementation equation becomes

$$\mathbf{u}=\mathbf{u_n}-\mathbf{QG_n^{-1}}(\mathbf{y}+\mathbf{n})+\mathbf{Qu} \tag{9}$$

where $\mathbf{y}+\mathbf{n}$ with $\mathbf{n}$ representing the sensor noise is used instead of $\mathbf{y}$ alone as this is the actual output signal that is available for feedback. This MIMO disturbance observer architecture is illustrated in the block diagram of Figure 1. Note that the choices (7) and (8) for the MIMO disturbance observer filters $\mathbf{Q}$ and $\mathbf{G_n^{-1}}$ result in m implementation equations. In this manner, the disturbance observer loops can be designed independently of each other with the purpose of loop i $(i=1,2,\ldots,m)$ being to achieve $u_i=G_{ni}u_{ni}$. The plant $\mathbf{G}$ is coupled and the effect of this coupling enters the individual disturbance observer compensated loops as a disturbance to be rejected.

Note that the multiplicative model uncertainty $\mathbf{\Delta_m}$ is used in the development of the MIMO disturbance observer and is a part of the extended disturbance $\mathbf{e}$ in Equations (4)–(6). However, this MIMO model uncertainty $\mathbf{\Delta_m}$ will not be used explicitly in the computational approach for parameter space solution that will be introduced later in the paper.

The equation relating the output $\mathbf{y}$ in Figure 1 to the command input $\mathbf{u_n}$, disturbance input $\mathbf{d}$ and the sensor noise input $\mathbf{n}$ is

$$\begin{aligned}\mathbf{y}=[\mathbf{I}+\mathbf{G}(\mathbf{I}-\mathbf{Q})^{-1}\mathbf{QG_n^{-1}}]^{-1}\{&\mathbf{G}(\mathbf{I}-\mathbf{Q})^{-1}\mathbf{u_n}\\&+\mathbf{d}-\mathbf{G}(\mathbf{I}-\mathbf{Q})^{-1}\mathbf{QG_n^{-1}n}\}\end{aligned} \tag{10}$$

The disturbance observer (9) has the two major functions of disturbance rejection and model regulation. Adequate sensor noise rejection is also desired. Consider the disturbance rejection transfer function matrix from disturbance input $\mathbf{d}$ to output $\mathbf{y}$ in (10) which can be converted into

$$\begin{aligned}&[\mathbf{I}+\mathbf{G}(\mathbf{I}-\mathbf{Q})^{-1}\mathbf{QG_n^{-1}}]^{-1}\\&\quad=\mathbf{I}-\mathbf{G}(\mathbf{QG_n^{-1}G}+\mathbf{I}-\mathbf{Q})^{-1}\mathbf{QG_n^{-1}}\end{aligned} \tag{11}$$

using the matrix inversion lemma (see Reference [7], for the matrix inversion lemma). Assuming $\mathbf{Q}(j\omega)=\mathbf{I}$ at low frequencies, the expression in (11) will become

Copyright © 2009 John Wiley & Sons, Ltd.

DOI: 10.1002/rnc

the zero matrix $\mathbf{0}$ meaning that the disturbance rejection goal is achieved for this choice of $\mathbf{Q}$.

Consider the model regulation transfer function matrix from command input $\mathbf{u_n}$ to output $\mathbf{y}$ in (10) which is desired to be $\mathbf{G_n}$ according to aim (3) at low frequencies. Use of the matrix inversion lemma followed by some manipulations transforms this transfer function matrix into

$$[\mathbf{I}+\mathbf{G}(\mathbf{I}-\mathbf{Q})^{-1}\mathbf{Q}\mathbf{G_n^{-1}}]^{-1}\mathbf{G}(\mathbf{I}-\mathbf{Q})^{-1} = \{(\mathbf{I}-\mathbf{Q})\mathbf{G}^{-1}+\mathbf{Q}\mathbf{G_n^{-1}}\}^{-1} \quad (12)$$

which becomes $\mathbf{G_n}$ when $\mathbf{Q}(j\omega)=\mathbf{I}$ is selected at low frequencies where model regulation is desired. Thus, the model regulation goal is achieved for $\mathbf{Q}(j\omega)=\mathbf{I}$. This ensures that the decoupled desired dynamics in $\mathbf{G_n}$ are achieved in the presence of the extended error $\mathbf{e}$ and is robust to plant modeling error $\mathbf{\Delta_m}$ and disturbances $\mathbf{d}$ which exist within $\mathbf{e}$.

Consider the sensor noise rejection transfer function matrix

$$-[\mathbf{I}+\mathbf{G}(\mathbf{I}-\mathbf{Q})^{-1}\mathbf{Q}\mathbf{G_n^{-1}}]^{-1}\mathbf{G}(\mathbf{I}-\mathbf{Q})^{-1}\mathbf{Q}\mathbf{G_n^{-1}} \quad (13)$$

from sensor noise input $\mathbf{n}$ to output $\mathbf{y}$. It should ideally be the zero matrix $\mathbf{0}$ at high frequencies. This disturbance rejection goal is achieved if $\mathbf{Q}(j\omega)=\mathbf{0}$ at high frequencies where sensor noise occurs. Thus, ideal disturbance observer operation requires $\mathbf{Q}(j\omega)=\mathbf{I}$ at low frequencies (model regulation and disturbance rejection) and $\mathbf{Q}(j\omega)=\mathbf{0}$ at high frequencies (sensor noise rejection). The choice of $\mathbf{Q}$ as a diagonal matrix of unity d.c. gain low pass filters as given in (8) satisfies these requirements at both low and high frequencies. In addition, note that $\mathbf{Q}(j\omega)=\mathbf{I}$ at both low and high frequencies should be avoided as this produces the additional two problems of assuming the exact knowledge of an uncertain plant and potential implementation issues related to inverting a known plant model.

With the addition of the feedback controller $\mathbf{C}$ to the disturbance observer compensated system in Figure 1, the block diagram in Figure 2 is obtained. The equation relating the reference input $\mathbf{r}$, the disturbance $\mathbf{d}$ and the sensor noise $\mathbf{n}$ to the output $\mathbf{y}$ becomes

$$\mathbf{y}=\{\mathbf{I}+\mathbf{G}(\mathbf{I}-\mathbf{Q})^{-1}(\mathbf{C}+\mathbf{Q}\mathbf{G_n^{-1}})\}^{-1}\{\mathbf{G}(\mathbf{I}-\mathbf{Q})^{-1}\mathbf{C}\mathbf{r} -\mathbf{G}(\mathbf{I}-\mathbf{Q})^{-1}(\mathbf{C}+\mathbf{Q}\mathbf{G_n^{-1}})\mathbf{n}+\mathbf{d}\} \quad (14)$$

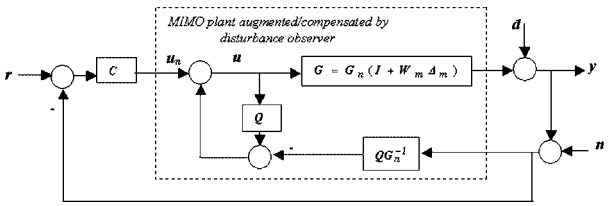

Figure 2. Plant under disturbance observer compensation and its feedback control.

Use of $\mathbf{Q}(j\omega)=\mathbf{I}$ at low frequencies results in ideal disturbance rejection; and reference command following corresponding to the disturbance observer augmented system in Figure 2 (within the dashed rectangle) being replaced by $\mathbf{G_n}$ at these frequencies. Use of $\mathbf{Q}(j\omega)=\mathbf{0}$ at high frequencies results in sensor noise rejection corresponding to the disturbance observer augmented system being replaced by the uncompensated plant $\mathbf{G}$ at these frequencies. This is the desired result which means that the disturbance observer compensated MIMO plant $\mathbf{G}$ can be replaced by the desired or nominal plant $\mathbf{G_n}$ within the bandwidth of the disturbance observer for the purpose of designing the feedback compensator $\mathbf{C}$ in Figure 2.

Note that the disturbance observer will not be able to decouple the loops at frequencies above its bandwidth. The Q_i filter bandwidths should therefore include frequencies of significant coupling between the loops.

The MIMO decoupled disturbance observer framework is a straightforward extension of the SISO formulation that enables the designer to reduce the MIMO design problem to several SISO design problems, with loop interactions being treated as disturbances. It is still quite useful and a natural choice for applications where one desires a decoupling of the loops that are considered, the car steering example used in this paper being one such case. This approach works well in practice, as the most significant feature of the disturbance observer architecture is its ability to reject disturbances within the bandwidth of the Q filter. The main assumption in this approach is that a decoupled dynamic behavior is wanted and that there are no loop interactions at higher frequencies outside the bandwidth of the Q filter which can at most be up to the actuator bandwidth for that loop. Another limitation of the proposed architecture

Copyright © 2009 John Wiley & Sons, Ltd.

DOI: 10.1002/rnc

is that only square MIMO systems can be handled. It is also assumed that the plant is stable to begin with. Otherwise a stabilizing controller has to be designed and used first.

3. DESIGN BY MAPPING FREQUENCY DOMAIN BOUNDS TO PARAMETER SPACE

The MIMO disturbance observer was introduced in the previous section. Design of the disturbance observer filter parameters by mapping selected frequency domain design bounds into disturbance observer filter parameter space is presented in this section. The SISO design approach is presented first. The MIMO design is handled by exploiting the decoupling nature of the MIMO disturbance observer introduced in Section 2 and applying loop-at-a-time SISO design.

The method that is presented here is based on the mapping of frequency domain constraints on closed-loop transfer functions like sensitivity, complementary sensitivity and mixed sensitivity into the parameter space of two selected controller parameters using a fixed structure controller. Several researchers have independently worked in this area of mapping various frequency domain criteria into parameter space. Some of the earlier work in this area can be found in References [8–16]. To the best of the authors' knowledge, the first use of one frequency at a time mapping of frequency domain constraints into controller parameter space has been carried out in [8]. In this approach, a frequency value is selected and ranges of values of two selected controller parameters in the structurally fixed controller that satisfy these criteria are solved for algebraically. Repetition of this procedure for a sufficient number of frequency points with subsequent display of the superposed solution region satisfying the constraint at all of the chosen frequencies results in a graphical characterization of the solution. This technique has been investigated for plants with real parameter uncertainty in [8]. A more systematic approach, utilizing, in principle the same technique, has been used in Reference [9] for mapping frequency domain constraints to PID controller parameter space. Application to the robust performance problem and use of a more general three term controller along with the PID controller structure are reported in [12, 13] where a CAD system for automated computation has also been presented. Similar results have also been reported in [10, 15] for a slightly more general, second-order controller structure. Limit cycle avoidance in parameter space has been developed in [11]. Nominal performance and robust stability-type frequency domain specifications were mapped into parameter space in [12]. The symbolic computation-based method in [12] was applied to a wide range of examples. An LMI formulation is used in [16] to obtain a solution to this problem for a fixed PID control structure, albeit not being able to handle plant dead time directly (Pade approximations are used). Out of these references, the formulation given below is similar to the one in [10].

The method presented here is one approach for robust control of MIMO systems and is based on the disturbance observer architecture. Note that several other methods for robust controller design that also impose structure on the plant model uncertainty or controller parameters exist. SSV-synthesis, for example, treats structured uncertainty and inevitably imposes structure on the design [17]. There is considerable research on linear parameter varying (LPV) systems analysis and LPV controller design with useful practical applications [18]. The edge-type results due to Barmish and the quantitative feedback theory work of Horowitz also impose some parameter-type structure on the final design [19, 20]. It is up to the designer to choose the method he prefers from the available literature.

3.1. SISO design

The parameter space design is based on satisfying the mixed sensitivity requirement

$$\| |W_S S| + |W_T T| \|_\infty < 1 \quad \text{or} \quad |W_S S| + |W_T T| < 1 \quad \text{for } \forall \omega \tag{15}$$

where $S := 1/(1+L)$ and $T := L/(1+L)$ are the sensitivity and complementary sensitivity transfer functions with L being the loop gain and W_S and W_T being the corresponding weights. Under the limit condition of the strict inequality in (17) becoming an equality, this

Copyright © 2009 John Wiley & Sons, Ltd.

DOI: 10.1002/rnc

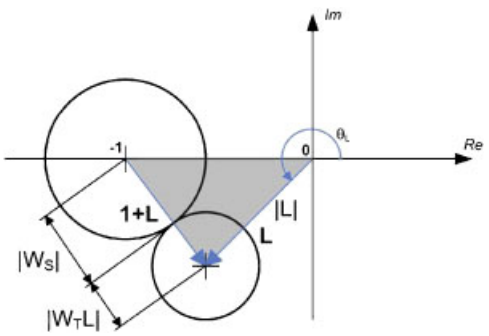

Figure 3. Illustration of the limit of the mixed sensitivity requirement for a specific frequency.

requirement can be represented as,

$$\left|\frac{W_S}{1+L}\right|+\left|\frac{W_T L}{1+L}\right|=1 \quad \text{or } |W_S|+|W_T L|=|1+L| \quad \text{for } \forall\omega \tag{16}$$

at each frequency. To obtain the region that satisfies (17) for all frequencies in the parameter space, (18) must be solved frequency at a time. The intersection of the regions for every calculated frequency results in the overall region being searched for. The graphical illustration of condition (18) is shown in Figure 3.

Applying the cosine rule to the shaded triangle in Figure 3, a graphical solution for $|L|$ results in,

$$|L|=\frac{-\cos(\theta_L)+|W_S||W_T|\pm\sqrt{\text{Disc}}}{1-|W_T|^2} \tag{17}$$

where

$$\text{Disc}=1+\cos^2\theta_L-2|W_S||W_T|\cos\theta_L +|W_S|^2+|W_T|^2 \tag{18}$$

when $L(\mathrm{j}\omega)$, $W_S(\mathrm{j}\omega)$ and $W_T(\mathrm{j}\omega)$ are used in Equations (17) and (18), the solutions for L at the chosen frequency ω are obtained. The solution procedure is to sweep angle θ_L from 0–2π rad (see [21], and the references therein for details for a standard feedback loop) and to solve for $|L|$ at each value of θ_L for which a solution exists. Then, all possible values of $L=|L|e^{\mathrm{j}\theta_L}$ at the chosen frequency ω are obtained. Each value of L satisfies

$$L=KG=(K_R+\mathrm{j}K_I)G \tag{19}$$

where K is the controller in an equivalent standard feedback architecture representation of the disturbance observer. The reader is referred to [21, 22] and the references therein for details of the general method of mapping frequency domain bounds to parameter space for a standard feedback control architecture. For the case of an SISO system with disturbance observer, the loop gain can be determined from Figure 1 as

$$L=\frac{GQ}{G_n(1-Q)} \tag{20}$$

Then, the disturbance observer parameters can be solved for frequency at a time and mapped into the parameter space for robust design of SISO systems with disturbance observer. For a specific structure defined as,

$$G_n=\frac{K_n(v)}{\tau_n s+1} \qquad Q=\frac{1}{\tau_Q s+1} \tag{21}$$

where $K_n(v)$ is the desired static gain of the disturbance observer-controlled system, the solution can be obtained by solving for τ_Q and τ_n from

$$K_R+\mathrm{j}K_I=\frac{L}{G}=\frac{Q}{G_n(1-Q)} \tag{22}$$

which results in the following symbolic solution:

$$\tau_Q=-\frac{1}{K_n K_I\omega} \qquad \tau_n=-\frac{K_R}{K_I\omega} \tag{23}$$

For more complicated, predefined structures of Q and G_n, the solution for τ_Q and τ_n exists and can be found by either searching for a symbolic solution of (22) or by solving it numerically. The end result is a region in a chosen controller parameter plane where the mixed sensitivity limit condition (18) is satisfied for the chosen frequency. Repetition of this procedure for a

Copyright © 2009 John Wiley & Sons, Ltd.

DOI: 10.1002/rnc

sweep of sufficiently many frequencies and superposition of the results by graphical intersection in the chosen parameter plane results in the overall solution region where the mixed sensitivity frequency domain bound is satisfied. The τ_Q–τ_n controller parameter plane is used for the choice (21) of disturbance observer filters.

3.2. MIMO design

A design based on mapping frequency domain bounds to parameter space can be carried out in a similar manner to the SISO case such that the MIMO system with the MIMO disturbance observer proposed in Section 2 is handled loop-at-a-time. In this case, the loop gain is,

$$\mathbf{L}=\mathbf{GK}=\mathbf{G}[\mathbf{I}-\mathbf{Q}]^{-1}\mathbf{Q}\mathbf{G}_\mathbf{n}^{-1} \tag{24}$$

Hence $\mathbf{K}$ is defined as,

$$\mathbf{K}=[\mathbf{I}-\mathbf{Q}]^{-1}\mathbf{Q}\mathbf{G}_\mathbf{n}^{-1}$$

Using (7) and (8)

$$\mathbf{K}=[\mathbf{I}-\mathbf{diag}(Q_i)]^{-1}\mathbf{diag}(Q_i)\mathbf{diag}\left(\frac{1}{G_{ni}}\right)$$

$$=\mathbf{diag}\left(\frac{Q_i}{G_{ni}(1-Q_i)}\right) \quad \text{for } i=1,\ldots,m \tag{25}$$

Thus, the ith element in the diagonal of $\mathbf{K}$ is

$$K_i=K_{Ri}+\mathrm{j}K_{Ii}=\frac{Q_i}{G_{ni}(1-Q_i)} \tag{26}$$

Assuming the basic structure,

$$G_{ni}=\frac{K_{ni}(v)}{\tau_{ni}s+1} \tag{27}$$

$$Q_i=\frac{1}{\tau_{Qi}s+1} \tag{28}$$

Similar to what was presented in the SISO case as Equations (23), the solution region for each frequency is given by

$$\begin{aligned}\tau_{Qi}&=-\frac{1}{K_{ni}K_{Ii}\omega}\\ \tau_{ni}&=-\frac{K_{Ri}}{K_{Ii}\omega}\end{aligned} \tag{29}$$

3.3. Using higher-order Q filters

The simplest possible disturbance observer Q_i filter is given by Equation (28). It is sometimes beneficial and sometimes necessary to use higher-order Q_i filters. For example, Q filters of the form

$$Q_{mn}(s)=\frac{\sum_{i=0}^{n}a_{mi}(\tau_Q s)^i}{(\tau_Q s+1)^m} \tag{30}$$

have been recommended for improved robustness in [23]. The coefficients a_{mi} in (30) can be found in that reference. The three Q filters given by,

$$Q_1(s):=Q_{10}(s)=\frac{1}{\tau_Q s+1} \tag{31}$$

$$Q_2(s):=Q_{21}(s)=\frac{2\tau_Q s+1}{(\tau_Q s+1)^2} \tag{32}$$

$$Q_3(s):=Q_{32}(s)=\frac{3(\tau_Q s)^2+3\tau_Q s+1}{(\tau_Q s+1)^3} \tag{33}$$

are used in the numerical example given in this paper to demonstrate the effect of higher-order Q filters on performance. It is possible that symbolic solutions may not exist or may be very lengthy for τ_Q and τ_n when higher filters of the form (30) are used. It is possible to solve the resulting equations numerically in such a case. Higher-order Q filters may be used in both the SISO and MIMO cases to enhance the robustness of the system.

4. ENHANCING SISO NOMINAL PERFORMANCE AND STABILITY

As the decoupling type of MIMO disturbance observer introduced in Section 2 can be designed loop-at-a-time using SISO design tools, SISO parameter space design enhancements for obtaining constant D-stability and desired phase margin regions in disturbance observer filter parameter space are presented in this section. Recall that multi-objective solutions are easily obtained by forming graphical intersections of several single-objective solutions in parameter space. The mixed sensitivity frequency domain bound objective of the previous section and the relative stability and phase

Copyright © 2009 John Wiley & Sons, Ltd.

DOI: 10.1002/rnc

margin bounds of this section can be combined to obtain a final overall solution region.

It is possible to further enhance the system stability and performance using the parameter space approach to robust control. Assuming perfect decoupling for the system, the SISO design methods given below can be applied to each loop for achieving better stability and performance of the MIMO system. The simple structure of a first-order filter for Q is assumed in this section, but it is possible to derive all the equations for higher-order filters as well.

4.1. Hurwitz stability

The system transfer function with the disturbance observer as given in Figure 1 can be written as,

$$\frac{y}{u_n} = \frac{G_n G}{G_n(1-Q)+GQ} \tag{34}$$

Assume that the plant is given by

$$\begin{aligned} G(s) &= \frac{N(s)}{D(s)} N(\mathrm{j}\omega) = N_R(\omega) + \mathrm{j}N_I(\omega) \\ D(\mathrm{j}\omega) &= D_R(\omega) + \mathrm{j}D_I(\omega) \end{aligned} \tag{35}$$

The closed-loop characteristic polynomial for the disturbance observer augmented system can then be obtained using (21) and (35) as follows:

$$\begin{aligned} \Delta p_{\mathrm{cl}}(s) &= K_n(v)\tau_Q s D(s) + N(s)(\tau_n s + 1) \\ &= a_{l+1}(\tau_Q, \tau_n, v)s^{l+1} + a_l(\tau_Q, \tau_n, v)s^l \\ &\quad + \cdots + a_1(\tau_Q, \tau_n, v)s + a_0(\tau_Q, \tau_n, v) \end{aligned} \tag{36}$$

where l is the degree of the plant $G(s)$. Note that the transfer functions G_n and Q may be different than the ones assumed in (36). The general method outlined here will not change. The Hurwitz stability boundary crossed by a pair of complex conjugate roots is characterized by the following equations:

$$\begin{aligned} &\mathrm{Re}[\Delta p_{\mathrm{cl}}(\mathrm{j}\omega)] = 0 \\ &\mathrm{Im}[\Delta p_{\mathrm{cl}}(\mathrm{j}\omega)] = 0 \quad \forall \omega \in (0, \infty] \end{aligned} \tag{37}$$

and there may be a real root boundary such that a single root crosses the boundary at $\omega = 0$ characterized by

$$\Delta p_{\mathrm{cl}}(0) = 0 \tag{38}$$

or

$$a_0(\tau_Q, \tau_n, v) = 0 \tag{39}$$

or there may exist an infinite root boundary which is characterized by a degree drop in the characteristic polynomial such that the coefficient of the largest power of the variable 's' happens to be zero. This degree drop in the closed-loop system polynomial is characterized as

$$a_n(\tau_Q, \tau_n, v) = 0 \tag{40}$$

Plotting the singular solutions of (39) and (40) in the parameter plane of τ_Q–τ_n together with the plot of (37) parameterized over ω and for a specific v value will yield the Hurwitz stability boundary and thus the Hurwitz stable region in the τ_Q–τ_n parameter space.

4.2. D-stability

The above Hurwitz stability parameter space region computation procedure can be extended to relative stability also called D-stability. For a system to be D-stable, the roots of the characteristic polynomial of the closed-loop system should lie in the D-stable region in the complex plane as shown in Figure 4. Note that the region in Figure 4 is one example of a type of D-stable region. D-stability regions are more general.

The boundary ∂_1 in Figure 4 can be mapped into the parameter space by substituting '$s-\sigma$' for 's' in (36) in order to shift the stability boundary to ∂_1 in the complex plane. Then solving for τ_Q and τ_n in (37) and

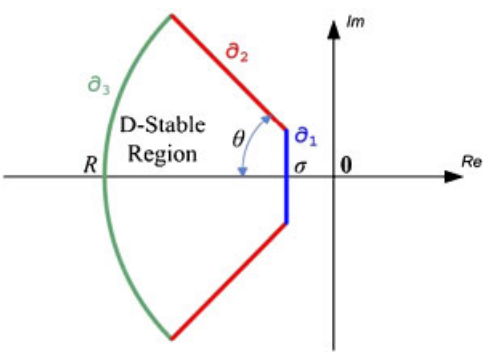

Figure 4. D-stable region in the complex plane.

Copyright © 2009 John Wiley & Sons, Ltd.

DOI: 10.1002/rnc

(39) in the same manner and plotting the result in the τ_Q–τ_n parameter plane will result in the ∂_1 boundary in the parameter space. Note that no infinite root boundary can exist since 's' is never equal to infinity in the D-shaped region of Figure 4. For mapping the boundary ∂_2 to the τ_Q–τ_n parameter plane, use '$re^{j\theta}$' for 's' in (36) and parameterize 'r' in Equation (38) to obtain the complex root boundary of ∂_1 after solving for τ_Q and τ_n. No singular solution exists since 'r' is never equal to zero or infinity. Finally, mapping the boundary ∂_3 to the τ_Q–τ_n parameter plane can be carried out by substituting 's' with '$Re^{j\theta}$' where 'R' is constant and parameterizing over 'θ' when solving (36). This results in the boundary ∂_3 in the parameter plane of τ_Q and τ_n after solving for these variables. For the choices (28) and (27) of Q and G_n, the real root boundaries of ∂_1, ∂_3 and the complex root boundaries of ∂_1, ∂_2, ∂_3 can be obtained symbolically in terms of τ_Q and τ_n.

4.3. Phase margin

The constant phase margin boundary can be plotted in the disturbance observer filter parameter space also. The constant phase margin boundary satisfies the following equation:

$$L(j\omega) = e^{j(m_\phi - \pi)} \tag{41}$$

where m_φ is the phase margin bound. The real and imaginary parts of $L(j\omega)$ can be expressed as

$$\begin{aligned}\mathrm{Re}[L(j\omega)] &= \mathrm{Re}\left[\frac{GQ}{G_n(1-Q)}\right] \\ &= \mathrm{Re}\left[\frac{N_R + jN_I}{D_R + jD_I}\frac{\tau_n j\omega + 1}{K_n \tau_Q j\omega}\right] \\ &= -\cos(m_\phi)\end{aligned} \tag{42}$$

$$\begin{aligned}\mathrm{Im}[L(j\omega)] &= \mathrm{Im}\left[\frac{GQ}{G_n(1-Q)}\right] \\ &= \mathrm{Im}\left[\frac{N_R + jN_I}{D_R + jD_I}\frac{\tau_n j\omega + 1}{K_n \tau_Q j\omega}\right] \\ &= -\sin(m_\phi)\end{aligned}$$

where the notation in (35) has been used for the plant G and the choices of disturbance observer filters (21) have been used. Equations (42) can also be expressed as

$$\begin{aligned}&\frac{D_R N_I - D_I N_R + (D_I N_I + D_R N_R)\tau_n \omega}{(D_R^2 + D_I^2) K_n \tau_Q \omega} \\ &\quad = -\cos(m_\phi) \\ &\qquad - \frac{D_I N_I + D_R N_R + (D_I N_R - D_R N_I)\tau_n \omega}{(D_R^2 + D_I^2) K_n \tau_Q \omega} \\ &\quad = -\sin(m_\phi)\end{aligned} \tag{43}$$

Then, solving for the parameters τ_Q and τ_n from (43) yields,

$$\begin{aligned}\tau_Q &= -\frac{N_I^2 + N_R^2}{K_n \omega (D_R N_I \cos(m_\phi) - D_I N_R \cos(m_\phi) - D_I N_I \sin(m_\phi) - D_R N_R \sin(m_\phi))} \\ \tau_n &= \frac{D_I N_I \cos(m_\phi) + D_R N_R \cos(m_\phi) + D_R N_I \sin(m_\phi) - D_I N_R \sin(m_\phi)}{\omega (D_R N_I \cos(m_\phi) - D_I N_R \cos(m_\phi) - D_I N_I \sin(m_\phi) - D_R N_R \sin(m_\phi))}\end{aligned} \tag{44}$$

as the equations for the constant phase margin region. Other choices of disturbance observer filters in Equations (42) can be handled in a similar manner. Note that the symbolic solutions may be too long in size for higher-order choices of these filters, necessitating a numerical solution. Constant gain margin region parameterization is also possible as it is obtained in a similar manner and is not presented here for the save of brevity.

5. REAL AND MIXED SSV ANALYSIS

While the disturbance observer design method presented is based on unstructured uncertainty, it is often the case that knowledge of parametric uncertainty in the system exists along with high-frequency

Copyright © 2009 John Wiley & Sons, Ltd.

DOI: 10.1002/rnc

unmodeled dynamics. It is then a good idea to use the design method in the paper and then to check for robust performance against this real parametric uncertainty and high-frequency unmodeled dynamics uncertainty using SSV analysis.

SISO and MIMO disturbance observer design procedures based on mapping the mixed sensitivity frequency domain bound, the relative D-stability constraint and the phase margin bound to disturbance observer filter parameter space were presented in previous sections. The mixed sensitivity frequency domain and phase margin specifications will result in the achievement of some level of stability and performance robustness in the presence of unstructured uncertainty. However, structured real parametric uncertainty in the plant is of importance in some problems and has to be dealt with explicitly, if this is the case. It is proposed to use real and mixed SSV analysis to check the stability and the performance robustness achieved by the multi-objective parameter space disturbance observer design method presented in this paper.

Real SSV is defined as (see Figure 5 with $\mathbf{\Delta_F = 0}$, $\mathbf{\Delta_m = 0}$)

$$\mu_{\mathbf{\Delta}_r}(\mathbf{N}) = \frac{1}{\min\limits_{\delta_i \in \Re; i=1,2,\ldots,n} \{(\max|\delta_i|) : \det(\mathbf{I} - \mathbf{N}\cdot\mathbf{diag}(\delta_1, \delta_2, \ldots, \delta_n)) = 0\}} \tag{45}$$

and is one over the size of the smallest destabilizing perturbation among the real parametric model uncertainty [21, 24]. $\mathbf{N}$ in (45) (see Figure 5) is the generalized plant in the linear fractional transformation form and $\Delta_r = \mathrm{diag}(\delta_1, \delta_2, \ldots, \delta_n)$ is the diagonal matrix of real parametric uncertainty with $\delta_i \in \Re; i = 1, 2, \ldots, n$. Real SSV can either be calculated by using results from the parametric approach to robust control or lower and upper bounds for it can be computed in the frequency domain approach to robust control. The latter approach is taken here as it is implemented in commercially available software [25]. In the SSV setting, the robustness of stability for a feedback system with $\|\Delta_r\|_\infty \leqslant 1$ is equivalent to satisfying

$$\sup_{\omega \in \Re} \mu_{\mathbf{\Delta}_r}(\mathbf{N}(\mathrm{j}\omega)) < 1 \tag{46}$$

High-frequency unmodeled dynamics that are present in all physical systems is modeled by a full complex uncertainty block and results in mixed SSV analysis (see $\mathbf{\Delta_m}$ and the weight $\mathbf{W_m}$ in Figure 5). The SSV-analysis technique is easily extended to handle the robustness of performance by treating the performance criterion as a fictitious, extra uncertainty block (see $\mathbf{\Delta_F}$ and the performance weight $\mathbf{W_S}$ in Figure 5). This extra uncertainty block is also complex and, along with high-frequency unmodeled dynamics, results in mixed SSV analysis where

$$\begin{aligned} \mu_{\mathbf{\Delta_r}, \Delta_m, \Delta_F}(\mathbf{N}_F) &= \frac{1}{\min\limits_{\delta_i \in \Re; i=1,2,\ldots,n; \Delta_m \in \mathbf{C}^{m \times m}, \Delta_F \in \mathbf{C}^{m \times m}} \{A\}} \\ A &= \{(\max(|\delta_1|, |\delta_2|, \ldots, |\delta_n|, |\Delta_m|, |\Delta_F|)) : \det(\mathbf{I} - \mathbf{N}_F \cdot \mathbf{B}) = 0\} \\ \mathbf{B} &= \mathbf{diag}(\delta_1, \delta_2, \ldots, \delta_n, \Delta_m, \Delta_F) \end{aligned} \tag{47}$$

is used for the computations.

Real SSV, in contrast to complex SSV, is plagued by its discontinuous nature as a function of frequency. It is, therefore, possible to miss the isolated real SSV peaks in a frequency sweep during computations. Both the treatment of the high-frequency unmodeled dynamics and the robust performance formulation requires the use of complex uncertainty blocks, resulting in what is known as the mixed SSV problem that combines at least one complex uncertainty block with the remaining real parametric uncertainty blocks. Mixed SSV is continuous with frequency, however, tall and narrow peaks that exist for mixed SSV may still be missed in a frequency sweep and one needs to be careful.

Copyright © 2009 John Wiley & Sons, Ltd.

DOI: 10.1002/rnc

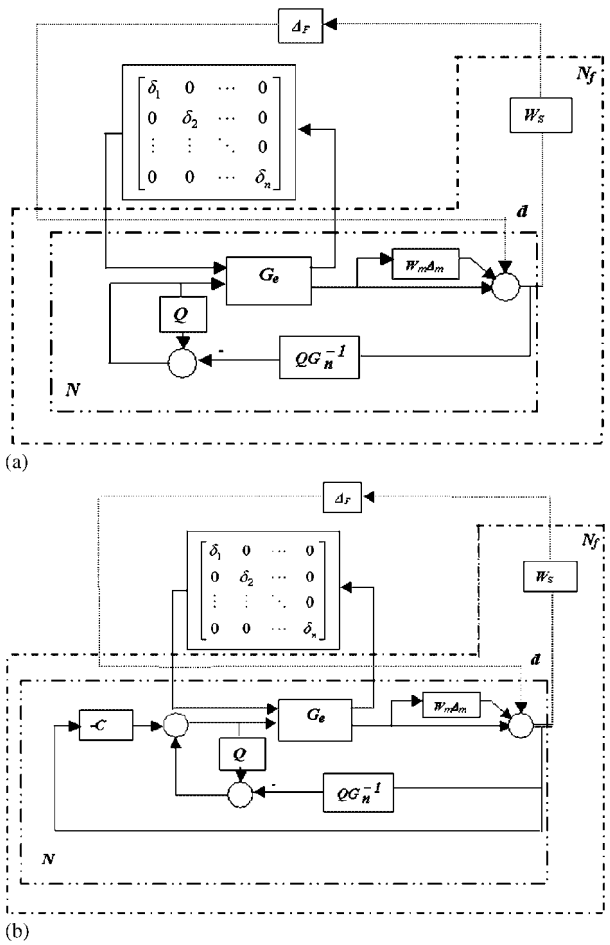

Figure 5. System with disturbance observer and structured uncertainty with: (a) no feedback controller and (b) feedback controller ($W_S = 0$ for robust stability).

Note that an SSV synthesis method could have been used for controller design also instead of the parameter space-based method presented in earlier sections. While the authors find SSV analysis to be very powerful for the analysis of structured uncertainty, the authors also believe in the strength of parameter space methods for design purposes, especially their interactive nature and the graphical display of results and that a solution region instead of a specific solution being the result of the design process. The main reasons for using the parameter space-based methods in the paper for design instead of SSV synthesis are: (1) a fixed controller structure and order can be used, (2) discontinuous, nonrational weights can be used, (3) time delays in the plant or poles on the imaginary axis pose no problems, and (4) the authors have used controllers resulting from similar parameter space design methods quite successfully in their previous applications. Regarding reason 1 given above, note that it may be possible to use a fixed controller structure in SSV-synthesis but the toolbox algorithm is known to be insensitive to real parameter variations in the mixed case, and may not even converge in the strictly real case. Hence, the resulting significant design conservatism would be a key disadvantage of an SSV-synthesis approach. Regarding reason 2 given above, the weights can be specified as magnitude bounds at chosen frequencies with zero phase angle. Regarding reason 3, the ability to handle plants with time delays is a major advantage of the proposed method as the SSV-synthesis method has difficulty in handling time delay.

6. APPLICATION TO EXAMPLE SYSTEM

A multi-objective parameter space approach for MIMO and SISO disturbance observer design was presented in Sections 2–4. A mixed SSV-based stability and performance robustness analysis approach for the designed SISO or MIMO disturbance observer was presented in Section 5. All of these results are applied to an MIMO example system, the four-wheel car steering application in this section.

6.1. Car steering model

The disturbance observer has been used successfully in robust steering controller design for vehicle yaw stabilization tasks ([5, 6, 26, 27], for example). This application of the disturbance observer is, thus, chosen as the example system. The single track model gives an accurate description of the lateral vehicle dynamics and is customarily used in steering controller design. The single track car model has been illustrated in Figure 6. The variables and parameters used in the single track model and their numerical values used in the computations are: F_{f} (lateral force at front wheel), F_{r} (lateral force at rear wheel), M_{zD} (yaw

Copyright © 2009 John Wiley & Sons, Ltd.

DOI: 10.1002/rnc

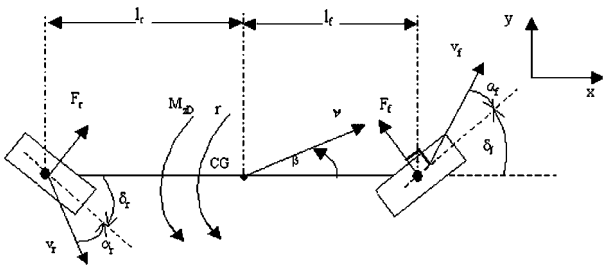

Figure 6. Single track car model.

disturbance moment), r (yaw rate), a_{fl} (lateral acceleration at front wheel), β (chassis side slip angle at vehicle center of gravity), v (magnitude of vehicle velocity at center of gravity, 30 m/s), l_{f} (distance from front axle to center of gravity, 1.25 m), l_{r} (distance from rear axle to center of gravity, 1.32 m), δ_{f} (front wheel steering angle), δ_{r} (rear wheel steering angle), m (vehicle mass, 1296 kg), J (moment of inertia wrt vertical axis at center of gravity, 1750 kgm^2), c_{f} (front wheel cornering stiffness, 84 000 N/rad), c_{r} (rear wheel cornering stiffness, 96 000 N/rad), μ (road-tire lateral friction coefficient, 1). The numerical values presented correspond to a mid-sized passenger car. In addition, the new variables $\tilde{m}=m/\mu$ and $\tilde{J}=J/\mu$ called the virtual mass and virtual moment of inertia are defined and customarily used in the model equations. The linearized single track car model is given by

$$\begin{bmatrix}\dot{\beta}\\ \dot{r}\end{bmatrix}=\begin{bmatrix}a_{11} & a_{12}\\ a_{21} & a_{22}\end{bmatrix}\begin{bmatrix}\beta\\ r\end{bmatrix}+\begin{bmatrix}b_{11} & b_{12}\\ b_{21} & b_{22}\end{bmatrix}\begin{bmatrix}\delta_{\mathrm{f}}\\ \delta_{\mathrm{r}}\end{bmatrix}$$
$$\begin{bmatrix}r\\ \beta\end{bmatrix}=\begin{bmatrix}0 & 1\\ 1 & 0\end{bmatrix}\begin{bmatrix}\beta\\ r\end{bmatrix}+\begin{bmatrix}0 & 0\\ 0 & 0\end{bmatrix}\begin{bmatrix}\delta_{\mathrm{f}}\\ \delta_{\mathrm{r}}\end{bmatrix} \tag{48}$$

where

$$a_{11}=-\frac{C_r+C_f}{\tilde{m}v},\quad a_{12}=-1+\frac{C_r l_r-C_f l_f}{\tilde{m}v^2}$$
$$a_{21}=\frac{C_r l_r-C_f l_f}{\tilde{J}},\quad a_{22}=-\frac{C_r l_r^2+C_f l_f^2}{\tilde{J}v}$$
$$b_{11}=\frac{C_f}{\tilde{m}v},\quad b_{12}=\frac{C_r}{\tilde{m}v},\quad b_{21}=\frac{C_f l_f}{\tilde{J}}$$
$$b_{22}=-\frac{C_r l_r}{\tilde{J}},\quad \tilde{m}=m/\mu,\quad \tilde{J}=J/\mu$$

The definitions of the other transfer functions in (48) are available in [22] and will not be presented as they will not be necessary in the following development. The state-space model (48) is an MIMO plant with front and rear wheel steering angles as its two inputs and with yaw rate and side slip angle as its two outputs.

Two uncertain parameters are identified as $\tilde{m}$ and v. They appear polynomially in the coefficients of the transfer functions obtained from the model (48). The MIMO disturbance observer design method in Section 3.2 is used with the four disturbance observer filters G_{n1}, G_{n2}, Q_1, Q_2 of the form (27) and (28). The loop-at-a-time design was carried out as presented in the earlier sections. The sensitivity function weight is chosen as

$$\mathbf{W_S^{-1}}(s)=\begin{bmatrix}h_{S1}\dfrac{s+\omega_{S1}l_{S1}}{s+\omega_{S1}h_{S1}} & 0\\ 0 & h_{S2}\dfrac{s+\omega_S l_{S2}}{s+\omega_{S2}h_{S2}}\end{bmatrix} \tag{49}$$

with $l_{S1}=0.5$ (i.e. less than 50% steady state error) being the low-frequency sensitivity bound, $h_{S1}=2$ being the high-frequency sensitivity bound and $\omega_{S1}=25$ rad/s being the approximate bandwidth of model regulation for the first loop. $l_{S2}=0.5$, $h_{S2}=4$ and $\omega_{S2}=3$ rad/s were used for the second loop.

The complementary sensitivity function weight is chosen as

$$\mathbf{W_T}(s)=\begin{bmatrix}h_{T1}\dfrac{s+\omega_{T1}l_{T1}}{s+\omega_{T1}h_{T1}} & 0\\ 0 & h_{T2}\dfrac{s+\omega_{T2}l_{T2}}{s+\omega_{T2}h_{T2}}\end{bmatrix} \tag{50}$$

where the low-frequency gain is $l_{T1}=0.2$ and the high-frequency gain is $h_{T2}=1.5$ (corresponds to uncertainty of up to 150% at high frequencies). The frequency of transition to significant model uncertainty is $\omega_{T1}=120$ rad/s for the first loop. $l_{T2}=0.2$, $h_{T2}=2$ with $\omega_{T2}=50$ rad/s were used for the second loop.

The first loop is from the front wheel steering angle to yaw rate and the second loop is from the rear wheel

Copyright © 2009 John Wiley & Sons, Ltd.

DOI: 10.1002/rnc

steering angle to vehicle sideslip angle. The cross-coupling effects of front wheel steering angle on vehicle sideslip angle and the rear wheel steering angle on yaw rate are treated as disturbances to be rejected. The decoupling-type MIMO disturbance observer in Section 2 and the design procedure in Section 3.2 result in two independent design procedures for the two loops of the four-wheel car steering system. The parameter space solution regions for these two loops are presented in Figures 7 and 8. The algorithm presented is a very fast numerical algorithm whose computation time depends on the number of grid points taken in the sweep of θ_L from 0 to 2π rad. Usually about 100 sweep points is taken for each frequency under consideration. The use of about 30 frequencies is sufficient to get a good characterization of the overall solution region per objective like D-stability, phase margin constraint, mixed sensitivity, etc. An SISO design takes on the order of fractions of a second on the computation platform that was used, comprising of an Apple MacBook with 2 GHz Intel Core with dual processors and 2 GB of RAM memory. A very large number of computation points (800 θ_L points and 100 frequency points, i.e. 80 000 repetitions of the basic computation) were used for the solution regions displayed in Figures 7 and 8 for better appearance of the results. This required a computational time of approximately 0.34 s. The MIMO design extension approach used contains one SISO design computation per MIMO loop considered. Computational scale thus increases linearly as $n \times t_{\mathrm{SISO}}$ where n is the number of MIMO loops and t_{SISO} is the computation time for each SISO loop in the MIMO system. Hence, for $n=2$, the computational time is approximately $2 \times 0.34\,\mathrm{s} = 0.68\,\mathrm{s}$.

The chosen disturbance observer filter parameter pairs are marked by crosses in these figures. The D-stable region and constant phase margin region plots for the first loop are given in Figures 9 and 10, respectively. The overall solution region for the first loop is obtained by graphical intersection of the solution region satisfying at least 80° phase margin and the regions in Figures 9 and 10 and is displayed in Figure 11. Since the MIMO design used is based on a decoupling approach forcing weakly coupled SISO loops, the PM mentioned above is for these desired SISO loops. The overall solution region for the second loop is displayed in Figure 12 for a D-stable region with $\sigma=3.5$, $\theta=60°$ and $R=30$ and a phase margin of at least 45°. The points marked with a cross in Figure 11 ($\tau_n=0.14\,\mathrm{s}, \tau_Q=0.04\,\mathrm{s}$) for the first loop and Figure 12 ($\tau_n=0.20\,\mathrm{s}, \tau_Q=0.06\,\mathrm{s}$) for the second loop are the disturbance observer filter parameters chosen and used in mixed SSV computations and in simulations.

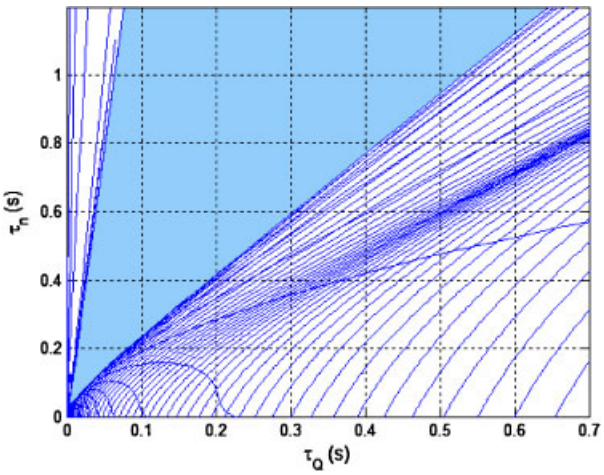

Figure 7. Front wheel to yaw rate loop solution region.

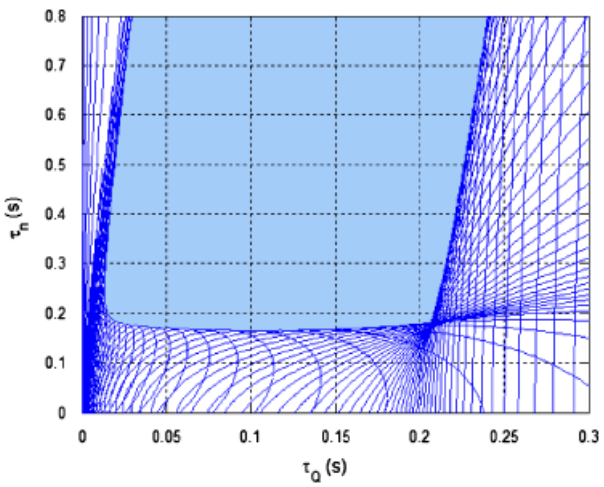

Figure 8. Rear wheel to side slip angle loop solution region.

Copyright © 2009 John Wiley & Sons, Ltd.

DOI: 10.1002/rnc

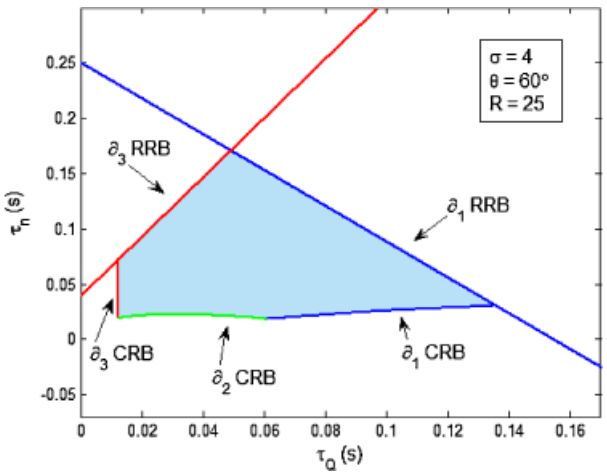

Figure 9. D-stable region for the first loop.

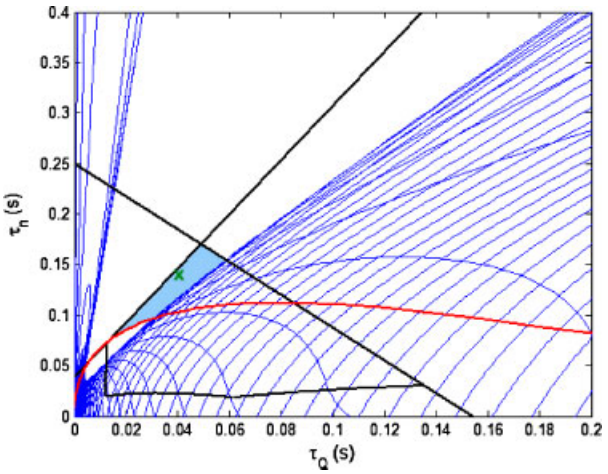

Figure 11. Overall solution region for the first loop.

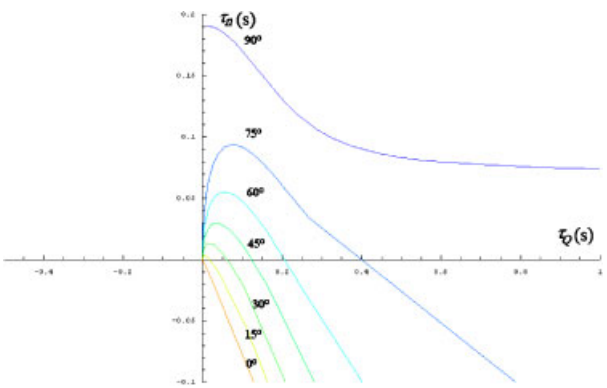

Figure 10. Constant phase margin plots for the first loop.

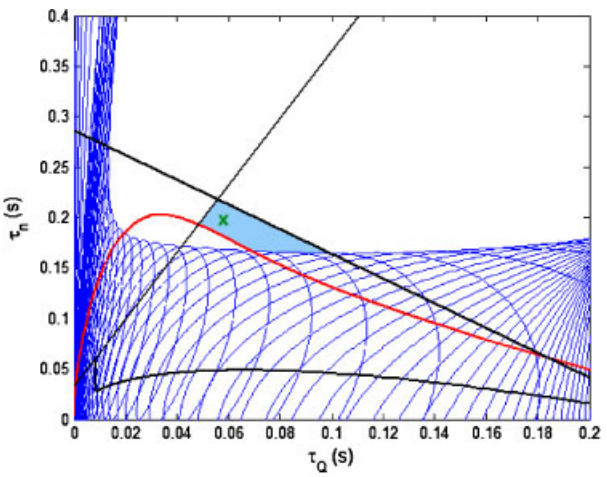

Figure 12. Overall solution region for the second loop.

The effect of the use of higher-order Q filters as given in (31)–(33) on the parameter space solution region for mixed sensitivity is shown in Figure 13.

Higher-order Q filters increase the area of the τ_Q–τ_n region for mixed sensitivity. Higher-order Q-filters are applied to the first loop only and the second loop is remained with the basic Q filter given by Equation (28). The solution regions are presented only for the first loop in the figure since the regions for the second loop remain the same. The solution region moves toward the right part of the controller parameter plane as the order of the Q filter is increased. One can choose lower τ_Q values and higher τ_n values by increasing the order of the Q filter while maintaining robust performance. When the D-stability criteria is also considered, moving in this direction in the τ_Q–τ_n plane moves the roots of the characteristic polynomial closer to the imaginary axis. Such an action introduces a slower response for the control system while maintaining robust performance. This can be desired in practice when the actuator bandwidth is low. But note that introducing higher-order Q filters makes the system less robust for higher frequencies. This tradeoff becomes essential when selecting the order of the Q filter for design. A good approach is to obtain the solution regions for a set of Q filters and then

Copyright © 2009 John Wiley & Sons, Ltd.

DOI: 10.1002/rnc

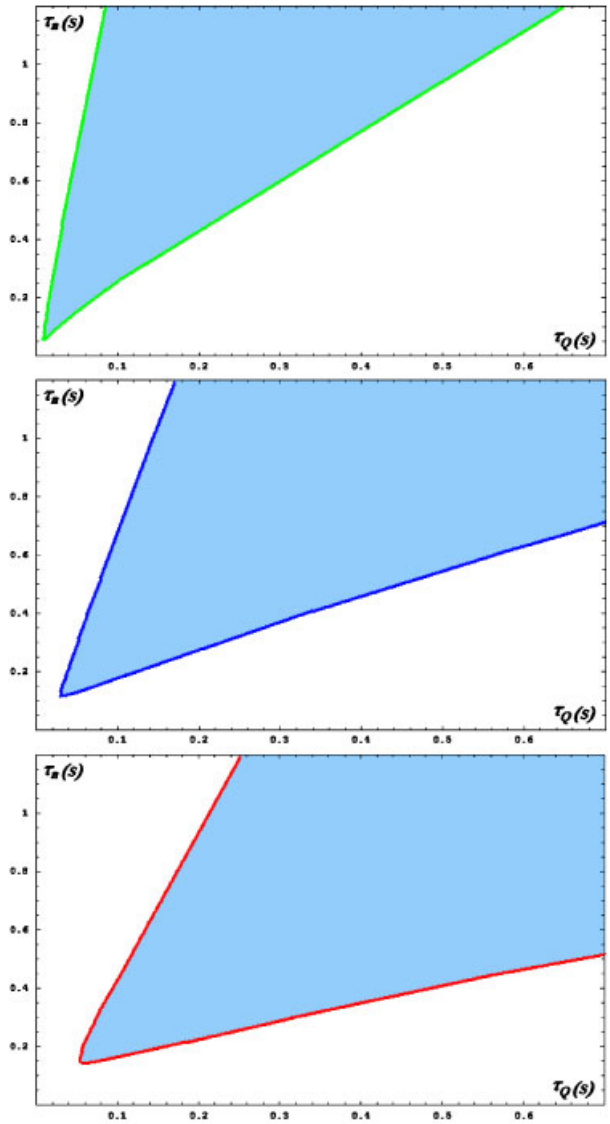

Figure 13. The solution region for the first loop when using higher-order Q filters for the first-order filter (top), second-order filter (middle), and the third-order filter(bottom).

select an order for the filter considering other parameter space criteria like D-stability and phase margin. Experimenting with different order Q filters is heuristic in nature and the results displayed in Figure 13 are problem dependent. It is a good idea for the designer

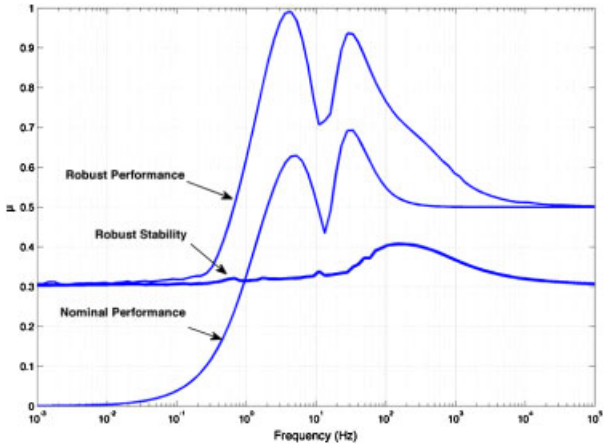

Figure 14. Result for the SSV analysis of the MIMO system.

to test a couple of Q filter choices to determine the one giving best results for his specific problem. The authors advise the use of the lowest-order Q filter that will get the job done for ease of controller implementation. But this is a choice that should be made by the designer.

An SSV analysis is carried out next. The actual plant with mixed real parametric and complex uncertainty and shown in Figure 6 is used. In the computations, $q_1 \equiv v$ and $q_2 \equiv \tilde{m}$ are the real uncertain parameters. $\Delta\tilde{m}$ and Δv are both chosen to reflect 30% uncertainty in the nominal values of $\tilde{m}$ and v. There is also a scalar complex uncertainty block used to represent high-frequency unmodeled dynamics. This is the complex uncertainty block Δ_m in Figure 5 where

$$W_m(s) = 3\frac{s + 2\pi \cdot 100 \cdot 0.1}{s + 2\pi \cdot 100 \cdot 3} \tag{51}$$

is used to represent 10 and 300% unmodeled dynamics uncertainty at low and high frequencies, respectively. The transition between low and high frequencies is chosen as 25 Hz in (51). The resulting SSV robustness plots are shown in Figure 14. As the maximum SSV value is smaller than unity, the robustness of stability and of performance are preserved for the model uncertainties considered. The use of higher-order Q filters as given in (31)–(33) results in Figure 15 for the SSV robustness results. These results show that higher-order Q filters increase SSV robustness at low frequencies at the cost of decreasing it at higher frequencies.

Copyright © 2009 John Wiley & Sons, Ltd.

DOI: 10.1002/rnc

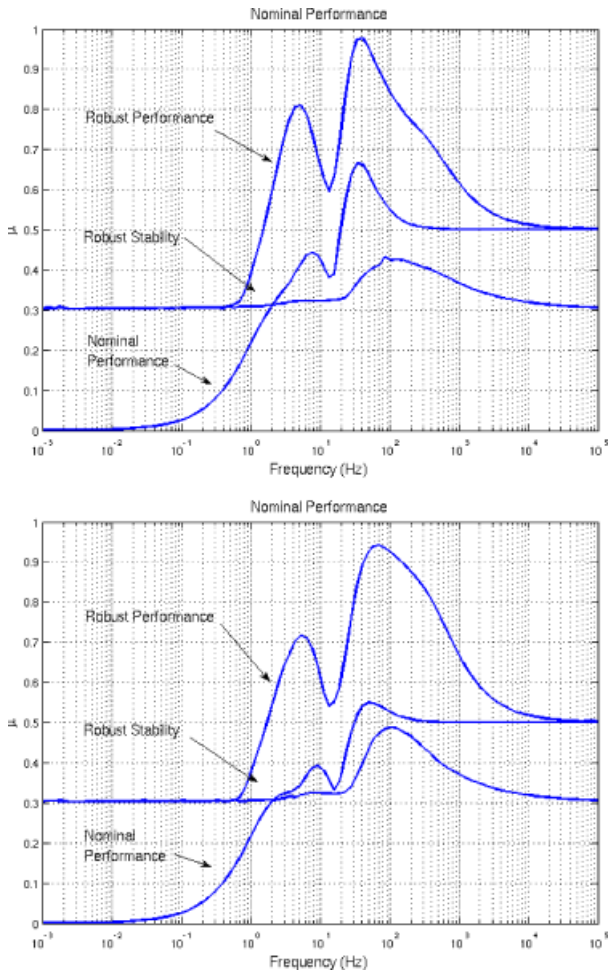

Figure 15. SSV results of higher-order Q filters used in the first loop for the second-order filter (top) and third-order filter (bottom) satisfying the SSV conditions.

7. SIMULATION STUDY

The simulations were carried out by inputting step front and rear wheel steering angles. The yaw rate output is shown in Figure 16. There is a yaw rate response to both front and rear wheel steering inputs in the uncontrolled case. The use of the MIMO disturbance observer introduced here results in a significantly decoupled response as the yaw rate responds mainly to the front wheel steering angle and only negligibly to the rear steering angle in the controlled case. The yaw rate response to front wheel step steering input behaves like the desired first-order system.

The simulation results from the steering angles to the vehicle side slip angle are shown in Figure 17. Note that high-frequency yaw rate sensor and vehicle side slip sensor noise were used in this simulation. The simulation results show that the MIMO disturbance observer had satisfactory noise rejection characteristics. Apart from the noise, the vehicle side slip angle responds mainly to rear wheel steering angle while it responds only negligibly to front wheel steering angle in the MIMO disturbance observer-controlled case, as expected. Yaw moment disturbance rejection simulations were also carried out and are shown in Figure 18. Excellent disturbance rejection is achieved with the MIMO disturbance observer as seen in Figure 18. Neither the yaw rate nor the vehicle side slip angle is affected much by yaw moment disturbances.

Two separate PID controllers were tuned for each loop of the car steering example (from front wheel steering to yaw rate and from rear wheel steering to side slip angle) and the resulting simulation results are also displayed in Figures 16–18 for benchmarking purposes. The PID loops were tuned manually with the result K_p=0.4, $K_i = 2\,\mathrm{s}^{-1}$, $K_d = 0.03\,\mathrm{s}$ for the first loop and $K_p = 0.7$, $K_i = 3.7\,\mathrm{s}^{-1}$, $K_d = 0.06\,\mathrm{s}$ for the second loop. It is seen from Figures 16–18 that desired model following is only achieved by careful tuning of PID gains, that decoupling of the two loops exists but is not as good as that of the MIMO disturbance observer. The Bode plots from the two inputs δ_f and δ_r to the two outputs r and β are shown in Figure 19. It is clear from Figures 16–19 that the PID-controlled plant has improved performance in relation to following the desired step response and improved disturbance rejection and decoupling of the loops as compared with the open-loop system. However, it is also seen that the loops are affected significantly by the dynamics of the other loop as decoupling is not as good as that of the MIMO disturbance observer.

8. CONCLUSIONS

A decoupling-type MIMO disturbance observer architecture was formulated here for square systems.

Copyright © 2009 John Wiley & Sons, Ltd.

DOI: 10.1002/rnc

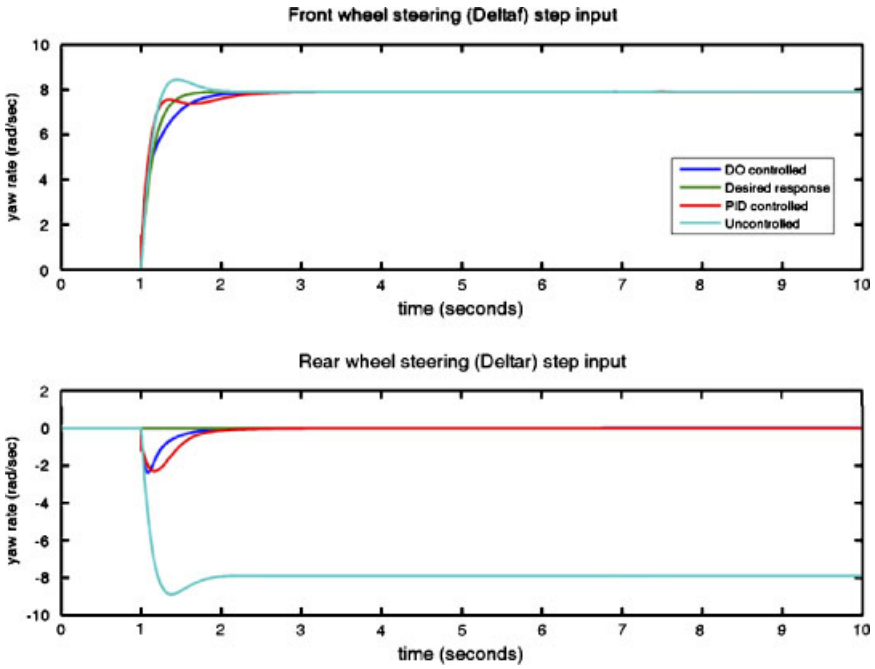

Figure 16. Step steering input simulation results for yaw rate output.

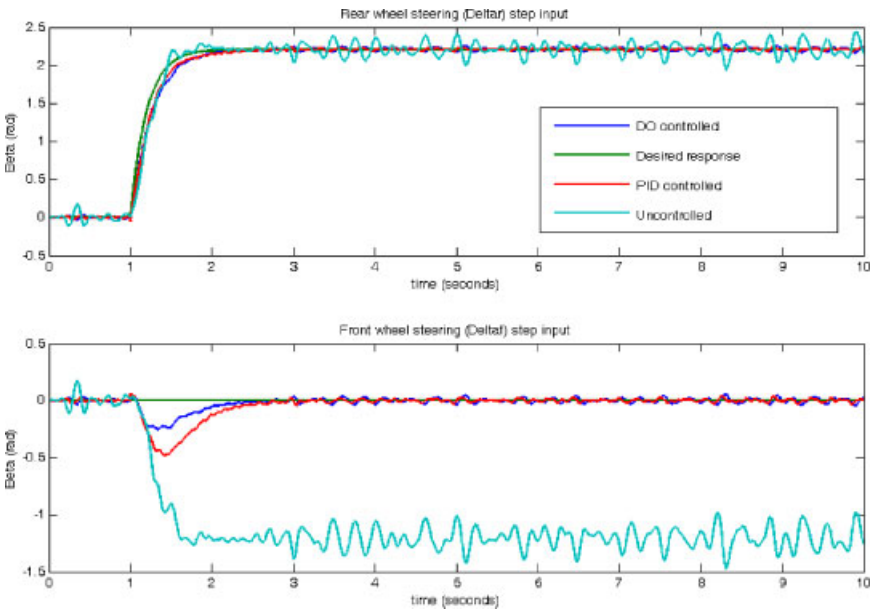

Figure 17. Step steering input simulation results for sideslip angle output with sensor noise.

Copyright © 2009 John Wiley & Sons, Ltd.

DOI: 10.1002/rnc

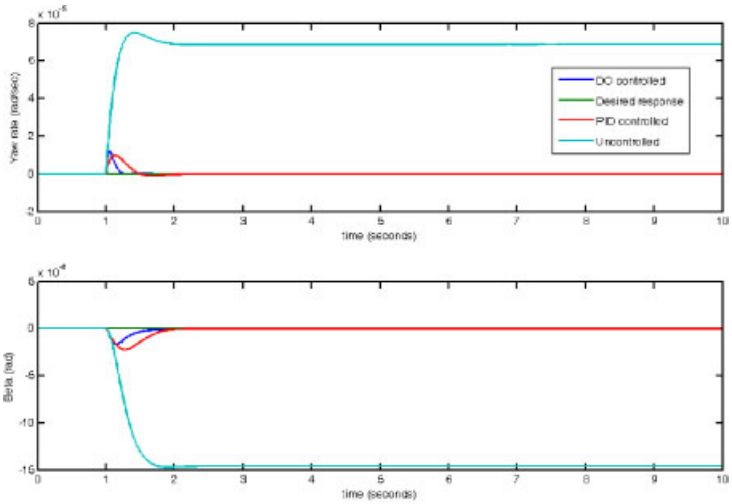

Figure 18. Step yaw moment input simulation results for yaw rate and sideslip angle outputs.

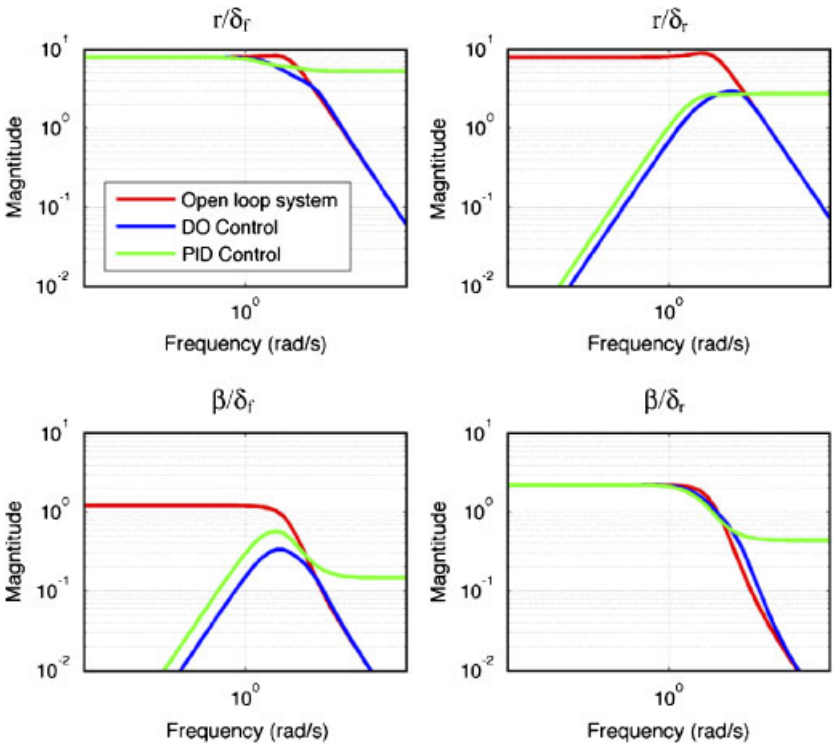

Figure 19. Model regulation and decoupling properties of MIMO disturbance observer and PID compensated system.

Copyright © 2009 John Wiley & Sons, Ltd.

DOI: 10.1002/rnc

A multi-objective parameter space disturbance observer design procedure satisfying certain D-stability, mixed sensitivity, and desired phase margin objectives was presented. For handling disturbance observer-compensated plants with significant amounts of real parametric uncertainty, the SSV analysis was proposed and used for analyzing stability and performance robustness. The effectiveness of the proposed methods was demonstrated by carrying out a design and simulation study for the four-wheel active steering control problem.

ACKNOWLEDGEMENTS

The authors acknowledge the support of the European Commission Framework Programme 6 through project INCO-16426.

REFERENCES

1. Ohnishi K. A new servo method in mechatronics. *Transactions of the Japan Society of Electrical Engineering* 1987; **107-D**:83–86.
2. Umeno T, Hori Y. Robust speed control of dc servomotors using modern two degrees-of-freedom controller design. *IEEE Transactions on Industrial Electronics* 1991; **38**(5):363–368.
3. Kempf CJ, Kobayashi S. Disturbance observer and feedforward design for a high-speed direct-drive positioning table. *IEEE Transactions on Control Systems Technology* 1999; **7**(5):513–526.
4. Güvenç L, Srinivasan K. Friction compensation and evaluation for a force control application. *Mechanical Systems and Signal Processing* 1994; **8**(6):623–638.
5. Aksun Güvenç B, Bünte T, Odenthal D, Güvenç L. Robust two degree of freedom vehicle steering compensator design. *IEEE Transactions on Control Systems Technology* 2004; **12**(4): 627–636.
6. Bünte T, Odenthal D, Aksun Güvenç B, Güvenç L. Robust vehicle steering control based on the disturbance observer. *IFAC Annual Reviews in Control* 2002; **26**(part 1):139–149.
7. Skogestad S, Postlethwaite I. *Multivariable Feedback Control Analysis and Design*. Wiley: New York, 1996.
8. Djaferis TE. Representations of controllers that achieve robust performance for systems with real parameter uncertainty. *Systems and Control Letters* 1991; **16**:329–339.
9. Saeki M. A design method of the optimal PID controller for a two disc type mixed sensitivity problem. *Transactions of the Institute of Systems*, *Control and Information Engineers* 1994; **7**(12):520–527.
10. Besson V, Shenton AT. Interactive control system design by a mixed $H\infty$-parameter space method. *IEEE Transactions on Automatic Control* 1997; **42**:946–955.
11. Bünte T. Beiträge zur robusten Lenkregelung von Personenkraftwagen. *Ph.D. Dissertation*, RWTH Aachen, VDI Fortschritt-Bericht, Reihe 12, Nr. 366, VDI-Verlag, Düsseldorf. 1998.
12. Odenthal D, Blue P. Mapping of H-infinity design specifications into parameter space. *Proceedings of the 3rd IFAC Symposium on Robust Control Design*, Prague, 2000.
13. Saeki M, Hirayama D. Parameter space design method of PID controller for robust sensitivity minimization problem. *Transactions of the Society of Instrument and Control Engineers* 1996; **32**(12):1612–1619.
14. Saeki M, Kimura J. Design method of robust PID controller and CAD system. *Proceedings of the 11th IFAC Symposium on System Identification*, vol. 3, Fukuoka, Japan, 1997; 1587–1593.
15. Saeki M. Fixed structure PID controller design for standard H-infinity control problem. *Automatica* 2006; **42**(1):93–100.
16. Besson V, Shenton AT. An interactive parameter space method for robust performance in mixed sensitivity problems. *IEEE Transactions on Automatic Control* 1999; **44**:1272–1276.
17. Yin G, Chen N, Li P. Improving handling stability performance of four-wheel steering vehicle via μ-synthesis robust control. *IEEE Transactions on Vehicular Technology* 2007; **56**: 2432–2439.
18. Biannic JM, Apkarian P. Missile autopilot design via a modified LPV synthesis technique. *Aerospace Science and Technology* 1999; **3**:153–160.
19. Barmish BR, Kang HI. A survey of extreme point results for robustness of control-systems. *Automatica* 1993; **29**:13–35.
20. Banos A, Horowitz I. QFT design of multi-loop nonlinear control systems. *International Journal of Robust and Nonlinear Control* 2000; **10**:1263–1277.
21. Güvenç L, Ackermann J. Links between the parameter space and frequency domain methods of robust control. *International Journal of Robust and Nonlinear Control* 2001; **11**(15): 1435–1453.
22. Ackermann J, Blue P, Bünte T, Güvenç L, Kaesbauer D, Kordt M, Muhler M, Odenthal D. *Robust Control*: *The Parameter Space Approach*. Springer: London, 2002.
23. Choi Y, Yang K, Chung WK, Kim HK, Suh IH. On the robustness and performance of disturbance observers for second-order systems. *IEEE Transactions on Automatic Control* **48**(2):315–320.
24. Zhou K, Doyle JC, Glover K. *Robust and Optimal Control*. Prentice-Hall: Englewood Cliffs, NJ, 1996.
25. *Robust Control Toolbox User's Guide*, The Mathworks, 2001.
26. Aksun Güvenç B, Güvenç L. The limited integrator model regulator and its use in vehicle steering control. *Turkish Journal of Engineering and Environmental Sciences* 2002; **26**:473–482.
27. Aksun Güvenç B, Güvenç L. Robust two degree of freedom add-on controller design for automatic steering. *IEEE Transactions on Control Systems Technology* 2002; **10**(1):137–148.

Copyright © 2009 John Wiley & Sons, Ltd.

DOI: 10.1002/rnc